





Statens vegvesen

Ferry free E39 -Fjord crossings Bjørnafjorden

304624

Rev.	Publish date	Description	Made by	Checked by	Project appro.	Client appro.
0	15.08.2019	Final issue	CAA	RML	SEJ	
Client	 Statens vegvesen					
Contractor	 Contract no.: 18/91094					

Document name:

**Preferred solution, K12 - Appendix E
Aerodynamics**

Document no.:

SBJ-33-C5-AMC-20-RE-105

Rev.:

0

Pages:

168

CONCEPT DEVELOPMENT, FLOATING BRIDGE E39 BJØRNAFJORDEN

Preferred solution, K12

Appendix E – Aerodynamics

CLIENT

Statens vegvesen

DATE: / REVISION: 15.08.2019 / 0

DOCUMENT CODE: SBJ-33-C5-AMC-20-RE-105



 **AAS-JAKOBSEN**  **COWI**  **Multiconsult**



 **AkerSolutions**

 entail

 NGI

 **DISSING+WEITLING**
architecture ajs

 **mossmaritime**

REPORT

PROJECT	Concept development, floating bridge E39 Bjørnafjorden	DOCUMENT CODE	SBJ-33-C5-AMC-20-RE-105
SUBJECT	Appendix E – Aerodynamics, K12	ACCESSIBILITY	Restricted
CLIENT	Statens vegvesen	PROJECT MANAGER	Svein Erik Jakobsen
CONTACT	Øyvind Kongsvik Nedrebø	PREPARED BY	Ketil Aas-Jakobsen
		RESPONSIBLE UNIT	AMC

SUMMARY

This document contains a summary of aerodynamic assessment of the K12 alternative for the Bjørnafjorden crossing. Further details are given in the notes in the reference list.

Aerodynamic coefficients, both static and flutter derivatives, was calculated by use of CFD. The CFD results were calibrated versus wind tunnel tests and take into account near ground effects for the low part of the bridge. For the high bridge part at zero degree angle of attack, Cd was found to be 0.68. Near ground effects increase these numbers by 20%. Traffic typically increased the drag factor with 70%. Aerodynamic coefficients is also given for cables (typically Cd=0.8), towers and columns (both typically Cd=1.5).

Recommendations for wind parameter input is given and is mainly based on N400 values. For parameters not given by N400, ESDU values are used.

The effect on the dynamic response of inhomogeneity in the wind due to aerodynamic forces has been studied in the frequency domain. Generally, maximum dynamic response is found for wind perpendicular to the main axis when the mean wind is uniformly distributed along the alignment. For cases with non-uniform distribution of mean wind, the dynamic response is smaller than for the case with uniform distribution.

Sensitivity to dynamic response was checked for P10, P50 and P90 values of the following wind parameters: xLu, Au, Cux and Cuy. For xLu values in medium range gave the highest response. For Au increased values gave increased response. For Cux and Cuy low values gave highest response.

The bridge system was checked for galloping, static divergence, classical flutter and torsion instability and it is found aerodynamically stable. A multimode approach was used when evaluating flutter, and the onset wind speed for flutter is calculated to be above 120m/s. Thus, fulfilling the criteria.

Vortex shedding is not expected for the bridge system.

To suppress cable vibrations external dampers are needed. The following phenomena was checked: Dry galloping, rain/wind galloping, ice/sleet galloping and vortex induced vibration.

It is recommended to perform detailed wind tunnel test before concluding on the girder cross sectional design and cable design.

The high turbulence of wind from the southern sector may lead to increased traffic closure of the bridge. We recommend that this is addressed in more detail.

0	15.08.2019	Final issue	K. Aas-Jakobsen	R. M. Larssen	S. E. Jakobsen
REV.	DATE	DESCRIPTION	PREPARED BY	CHECKED BY	APPROVED BY

TABLE OF CONTENTS

1	Introduction.....	5
2	Aerodynamic coefficients.....	6
2.1	Bridge deck	6
2.2	Wind tunnel tests. How to use the results in design.	6
2.3	Aerodynamic load coefficients for K12	7
2.4	Bridge deck for K12 –design values.	8
2.5	Cables.....	9
2.6	Square element. Columns and pylons.	9
2.7	Pontoons.....	10
3	Wind input.....	10
3.1	Introduction	10
3.2	Recommendation for wind input in design.....	11
3.3	Inhomogeneity in wind – simplified model benchmarking.....	11
3.4	Inhomogeneity in wind - mean wind variation along the alignment	14
3.5	Effects of varying wind parameters.	15
4	Aerodynamic stability	17
4.1	Introduction – evaluation of bridge girder aerodynamic properties.	17
4.2	Vortex induced vibrations.....	17
4.3	Verification of aerodynamic instability	18
4.3.1	Galloping.....	18
4.3.2	Static divergence.....	18
4.3.3	Classical flutter.....	19
4.3.4	Torsion instability.....	20
4.4	Evaluation of flutter coefficients used.....	21
4.5	Tower.....	21
4.6	Vibration of cables in the cable stayed bridge.....	21
4.6.1	Introduction	21
4.6.2	Dynamic properties and external damping for cables.	22
4.6.3	Dry galloping	23
4.6.4	Galloping from surface irregularities of HDPE tube	24
4.6.5	Rain/wind galloping	26
4.6.6	Ice/sleet galloping.....	26
4.6.7	Vortex induced vibrations.....	28
5	Other wind related issues	29
5.1	Bridge closure due to wind	29
6	References.....	30
7	Enclosures	31

1 Introduction

Several floating bridge concepts are proposed for the Bjørnafjorden crossing. This document explore the effect of aerodynamics on the K12 concept, which is the curved bridge with side anchors as shown in Figure 1.

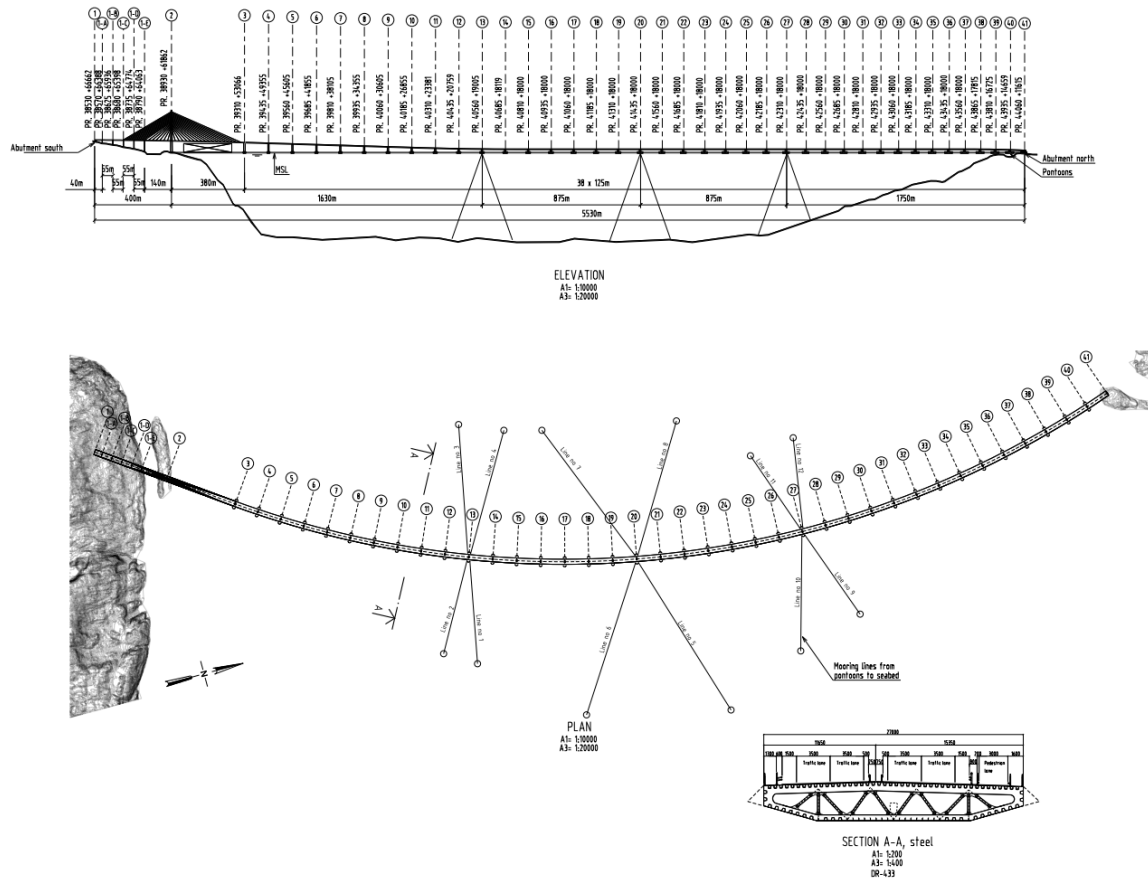


Figure 1 K12 General arrangement.

Aerodynamic assessment of the Bjørnafjorden K12 concepts has focused on the following tasks:

1. Derive aerodynamic load coefficients for the relevant cross sections. For the most important cross section, the stiffening girder, a CFD analysis was performed. The coefficients are calibrated towards the wind tunnel tests and used as input to the analysis.
2. Perform aerodynamic stability analysis of K12 to assure that the behavior of the bridge is predictable.
3. Assess the effect on dynamic response of the bridge due to variation of wind parameters along the alignment (i.e. inhomogeneity of wind).
4. Identification of other aerodynamic phenomena which can impact the design or operability of the structure.

2 Aerodynamic coefficients

2.1 Bridge deck

The bridge deck is a continuous aerodynamic stiffening girder in steel starting at the high bridge in south and continuing down the ramp and along the low part of the bridge to the north abutment. A length of more than 5300m. A principle cross section with definition of Drag, Lift and Moment coefficients is shown in Figure 2, while the K12 cross section is shown in Figure 5.

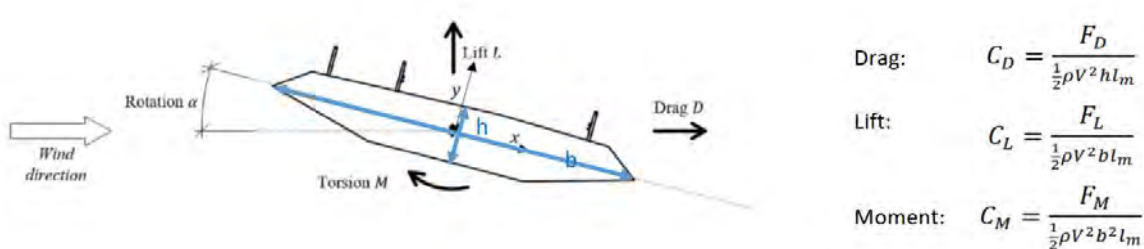


Figure 2 Aerodynamic definitions.

2.2 Wind tunnel tests. How to use the results in design.

The wind tunnel tests were conducted in several configurations and is reported in [2]. Among them were a normal test, where the test specimen is unaffected by the wind tunnel boundary, a test where the cross section is about 14m in full scale from bottom of the wind tunnel and test with traffic.

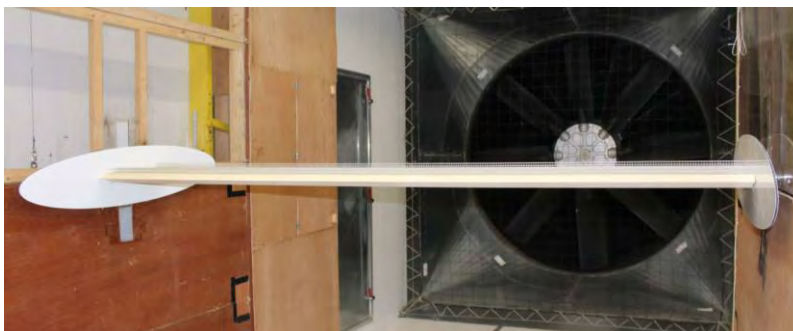


Figure 3 Example of wind tunnel test without surface boundary.

The main findings and how it is implemented in design is shown in Table 1:

Table 1 Wind tunnel tests: Conclusions and how it is implemented in design.

Conclusion	How it is implemented in design
The flat free-surface boundary increases drag by approx. 10-20 %	The flat free surface boundary drag value used in the analysis is based on results from CFD analysis calibrated towards the wind tunnel tests. For the low part of the bridge only C_D is increased with 20% to account for near surface effects. For the ramp part and high bridge near

	surface boundary effects is not taken into account.
The traffic box increases drag by approx. 30-40 % for western winds and approx. 60-70 % for eastern winds. Note that the traffic box is always positioned on the upstream side of the road deck.	The difference from eastern and western wind is most likely due to the position of the pedestrian walkway. In this stage it is chosen to not take this into account. Drag factors with traffic is increased by 70%.
The traffic box decreases the lift and moment slopes.	This is not taken into account in the factors used for traffic and is conservative.

2.3 Aerodynamic load coefficients for K12

In order to be able to understand the aerodynamic effects on the cross section, CFD analysis were performed with the built in tool in RM bridge. As an initial step the CFD tool was calibrated towards the wind tunnel tests already performed /2/.

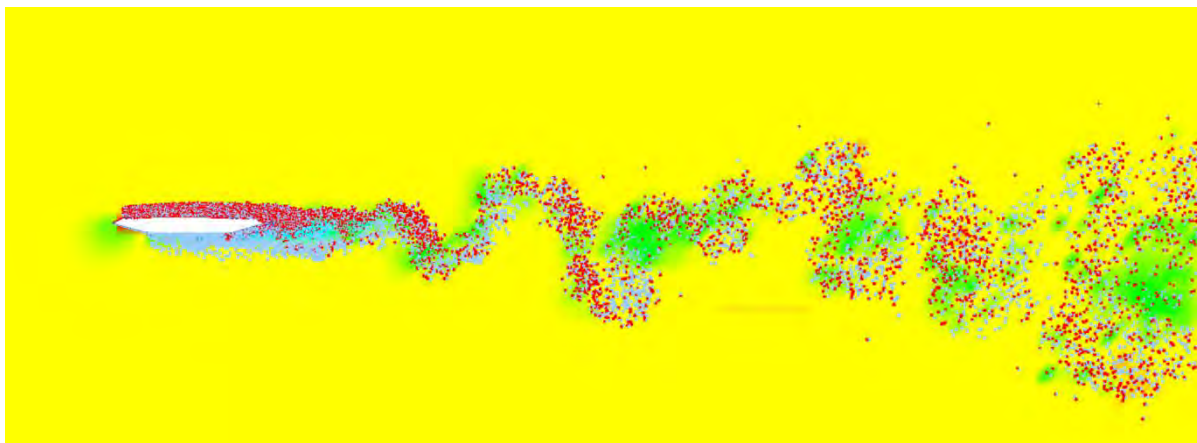


Figure 4 Example of output from CFD analysis.

Figure 4 gives an impression of the output from the CFD tool. For the K12 option wind load coefficients and aerodynamic derivatives are given in /16/. The resulting aerodynamic derivatives for K12 is given in Figure 6.

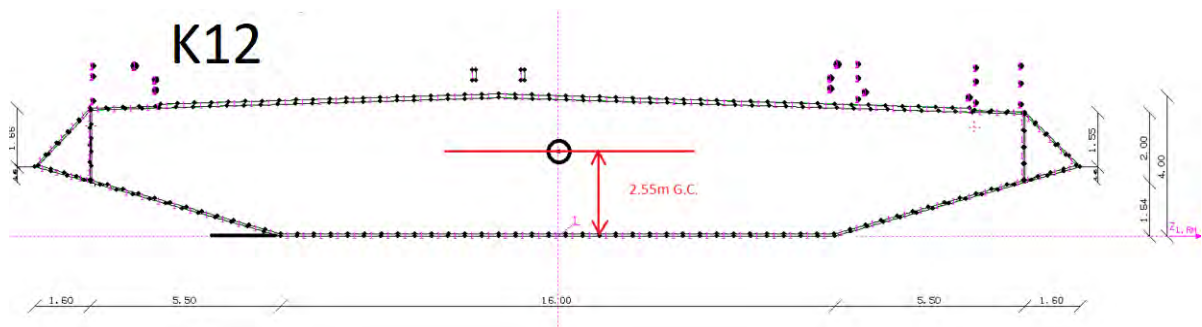


Figure 5 Discrete vortex panel model of the K12 cross section geometry.

2.4 Bridge deck for K12 –design values.

The proposed aerodynamic coefficients given below is based on calibrated wind tunnel tests and extrapolated results from the CFD investigations and represents an envelope of the most unfavourable results. Table 1 is used to derive the aerodynamic drag coefficients for the near surface and traffic cases. The values are derived for turbulent wind and a deck height of 4.0m. For the traffic cases the reference height is the height of the bridge deck without the traffic box.

The values given in Table 2 is used in the integrated analysis. For the high bridge part at zero degree angle of attack Cd was found to be 0.68 for the aerodynamic box girder. For the low bridge near ground effects were taken into account, which increase the numbers by about 20% to 0.82. Traffic typically increased the drag factor with 70%.

Aerodynamic derivatives of K12 obtained from CFD analysis is given in Figure 6.

It is recommended to do wind tunnel test to obtain more accurate values for the final cross section.

Table 2 Aerodynamic load coefficients used in integrated analysis.

AOA [deg]	AOA [rad]	Cd [] HB	Cd [] HB/wT	Cd [] LB	Cd [] LB/wT	Cl []	dCl [] [1/rad]	Cm []
-8,00	-0,140	1,261	2,144	1,513	2,572	-0,941		0,110
-5,00	-0,087	0,883	1,501	1,060	1,801	-0,731	4,148	0,069
-3,00	-0,052	0,752	1,278	0,902	1,534	-0,579	4,502	0,033
-1,50	-0,026	0,699	1,188	0,839	1,426	-0,456	3,839	0,007
0,00	0,000	0,681	1,158	0,817	1,389	-0,378	3,247	-0,019
1,50	0,026	0,672	1,142	0,806	1,371	-0,286	3,667	-0,045
3,00	0,052	0,687	1,168	0,824	1,401	-0,186	3,487	-0,067
5,00	0,087	0,766	1,302	0,919	1,563	-0,073	2,727	-0,096
8,00	0,140	0,909	1,545	1,091	1,854	0,052		-0,125

HB=High Bridge, LB=Low Bridge, wT=with Traffic, ALL=valid for whole bridge

Coefficients derived for turbulent flow.

For the traffic cases the reference height is the height of the bridge deck without the traffic box

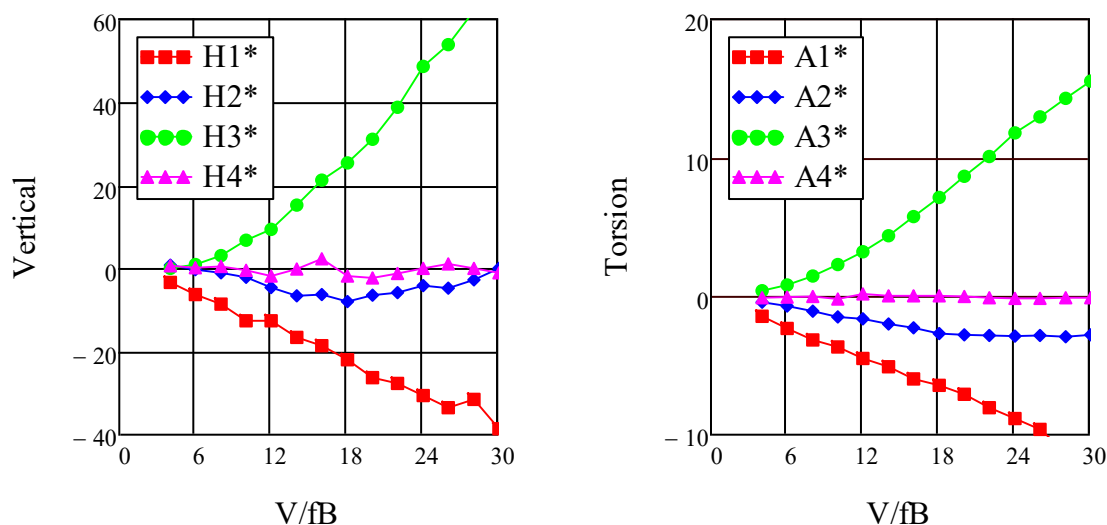


Figure 6 Aerodynamic derivatives for the K12 cross section from discrete vortex simulations.

2.5 Cables

The drag factor for cables is calculated from /3/ based on a diameter of 200mm. If the diameter of the cables deviates significantly from this a reevaluation is necessary

Table 2 Drag coefficients for cables. Reference length is diameter of cable.

Mean wind speed	Cd
Less than 20 m/s	1.2
Above and including 20m/s	0.8

2.6 Square element. Columns and pylons.

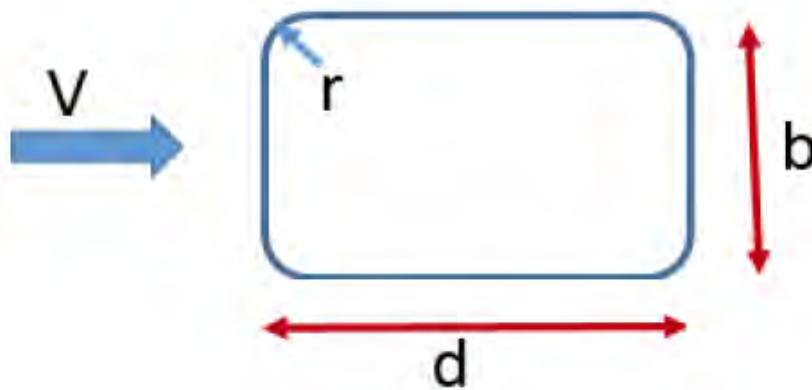


Figure 7 Definitions for drag factor of rectangular cross section.

The suggested values is calculated from /3/ and is based on a corner cut of $r=0.7m$ and a drag value of 1.5 was used for all aspect ratios. This is conservative for the selected corner cut, see Figure 4 for definitions and Figure 5 for result of calculations.

Shielding effects is not taken into account. Lift and moment coefficients are currently set to zero.

Drag factor columns and pylons: $C_d = 1.5$

Forces is calculate based on b: e.g. $F=0.5 \cdot \rho \cdot C_d \cdot b \cdot V^2$

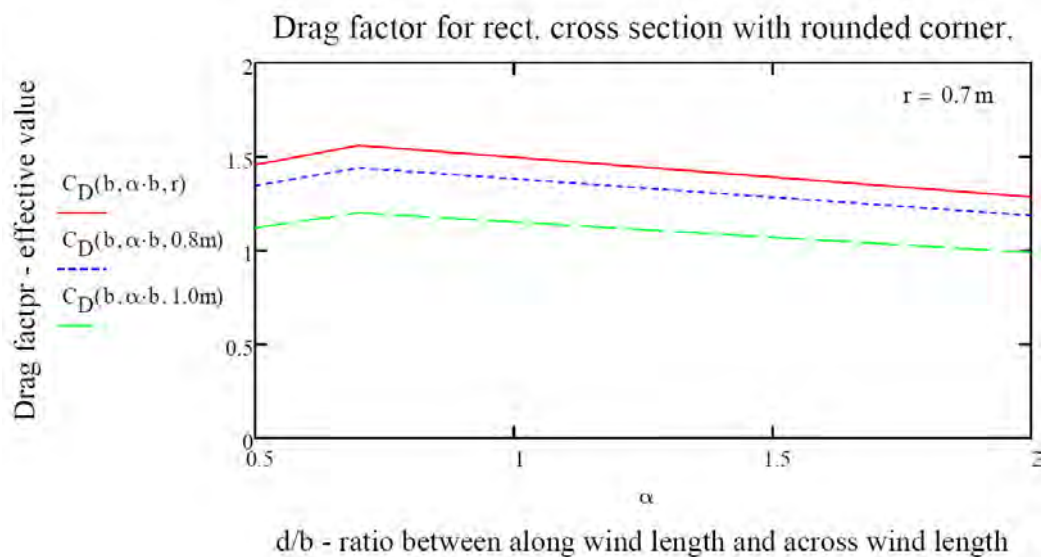


Figure 8 Drag factor for rectangular cross section with rounded corner

Aerodynamic load coefficients for the tower in the cable stayed bridge is given in Amendment A of this document. The factors are based on NS-EN-1991-1-4:2005 §7.6 /5/. In addition shielding is taken into account and the shielding effect is taken from wind tunnel tests of a reference project.

2.7 Pontoons

See appendix F for applied wind loading on pontoons.

3 Wind input

3.1 Introduction

Chapter 2 in the Metocean Design basis /2/ give details about how the wind shall be defined for the structure and is based on a wind measurement campaign at the bridge site. Among other things it specifies a variation of the magnitude of the mean wind speed along the alignment and gives range of possible variations of wind parameters.

Table 15 in the Metocean Design Basis gives information about the variation of wind parameters. These are based on site measurements. As can be seen, there are quite large variations and it is not immediately clear what will govern the design. During the design process it was, together with SVV, decided to perform the design according to N400 values, with some additional sensitivity studies. This section contain analysis describing the effect of changing different parameters in the wind.

The parameters shown will affect the magnitude of the wind spectrum, where the peak is positioned along the frequency axis and how it tapers off at higher frequencies. Thus, the choice of which parameters to use may affect the outcome of the wind response

Table 3 Wind spectra and coherence, updates received 18.03.2019. According to clarification 304624-1-A-0041 N400 values are used in design.

Parameter	N400	P10	P50	P90
xL_u	162 m	108 m	232 m	586 m
xL_v	40.5 m	50 m	141 m	472 m
xL_w	13.5 m	21 m	40 m	81 m
yL_u	54.0 m	X	X	X
yL_v	40.5 m	X	X	X
yL_w	9.0 m	X	X	X
zL_u	32.4 m	X	X	X
zL_v	13.5 m	X	X	X
zL_w	9.0 m	X	X	X
A_u	6.8	3.9	7.3	16.3
A_v	9.4	5.6	13.3	32.5
A_w	9.4	7.7	12.3	18.2
C_{uy}	10.0	6.4	8.0	10.8
C_{uz}	10.0	8.3	11.5	17.6
C_{vy}	6.5	3.0	3.8	4.9
C_{vz}	6.5	6.0	8.8	16.5
C_{wy}	6.5	4.5	5.8	8.3
C_{wz}	3.0	2.8	3.7	5.7

3.2 Recommendation for wind input in design

Wind input is taken from N400. Where N400 does not give any indications, ESDU is used.

*Table 4 Recommended wind input for analysis.
According to clarification 304624-1-A-0041 N400 values are used in design.*

Parameter	Z=10m	Z=50m	P-level
xLu [m]	100,0	162,1	N400
xLv [m]	25,0	40,5	N400
xLw [m]	8,3	13,5	N400
Au	6,8	6,8	N400
Av	9,4	9,4	N400
Aw	9,4	9,4	N400
Cux (*)	3,0	3,0	N400
Cuy	10,0	10,0	N400
Cuz	10,0	10,0	N400
Cvx (*)	6,0	6,0	N400
Cvy	6,5	6,5	N400
Cvz	6,5	6,5	N400
Cwx (*)	3,0	3,0	N400
Cwy	6,5	6,5	N400
Cwz	3,0	3,0	N400

(*) Not given in design basis – N400 or ESDU values used.

The following wind data is also used in the analysis:

Roughness length, $z_0 = 0.01$

Terrain factor, $k_T = 0.17$

1h mean wind speed with return period 100 years: 29.6 m/s.

In Windsim, which is used to generate coherent wind time series, the basic wind speed, v_b , is used as input. The basic wind speed for 1h mean wind with a return period of 100 years with the above parameters is (§4.3.2 in /5/):

$$v_b = v_m(z)/c_r(z), \text{ where } c_r(z) = k_T \cdot \ln(z/z_0) = 1.173 \text{ and } v_m(10m) = 29.6 \text{ m/s} \Rightarrow v_b = 29.2\text{m/s} / 1.1173 = 25.2 \text{ m/s}$$

For the turbulence the following is used to calculate I_v and I_w based on I_u . This differs from N400 default, and thus, the input must be adjusted with the following scale factors in Windsim:

$$I_v = 0.84 I_u. \Rightarrow \text{Windsim scale factor} = 0.84/0.75 = 1.12$$

$$I_w = 0.60 I_u. \Rightarrow \text{Windsim scale factor} = 0.6/0.5 = 1.20$$

3.3 Inhomogeneity in wind – simplified model benchmarking

The analysis was conducted for wind response only. It was selected to use wind speed with 100year return period and as a first step it was selected to calculate response with the same turbulence intensity for all directions. Thus, standard N400 formulas and values are used in these reference calculations and the wind input to the analysis is:

Basic wind speed at z=10m : $v_b=25.2\text{m/s}$

Surface roughness: $z_0=0.01$

Length scale at z=10m: $xLu=100\text{m}$

Spectral shape parameter: $Au=6.8$

Decay parameters: $Cux=3, Cuy=10, Cuz=10$

Results are calculated for all angles of attack and presented as standard deviation of transverse displacement in a polar diagram.

The analysis is performed with a simplified frequency domain method implemented in Python. Thus, giving a high level of flexibility of implementing new features. The main simplifications is on the load model, it is linearized, and that only the resonant part of the response is included. When the background part of the response is include the standard deviation increases with about 6% compared to what is reported herein. In the simplified method the response is calculated for the first 20 modes, shown in Figure 9, which contain plots of the first 30 modes.

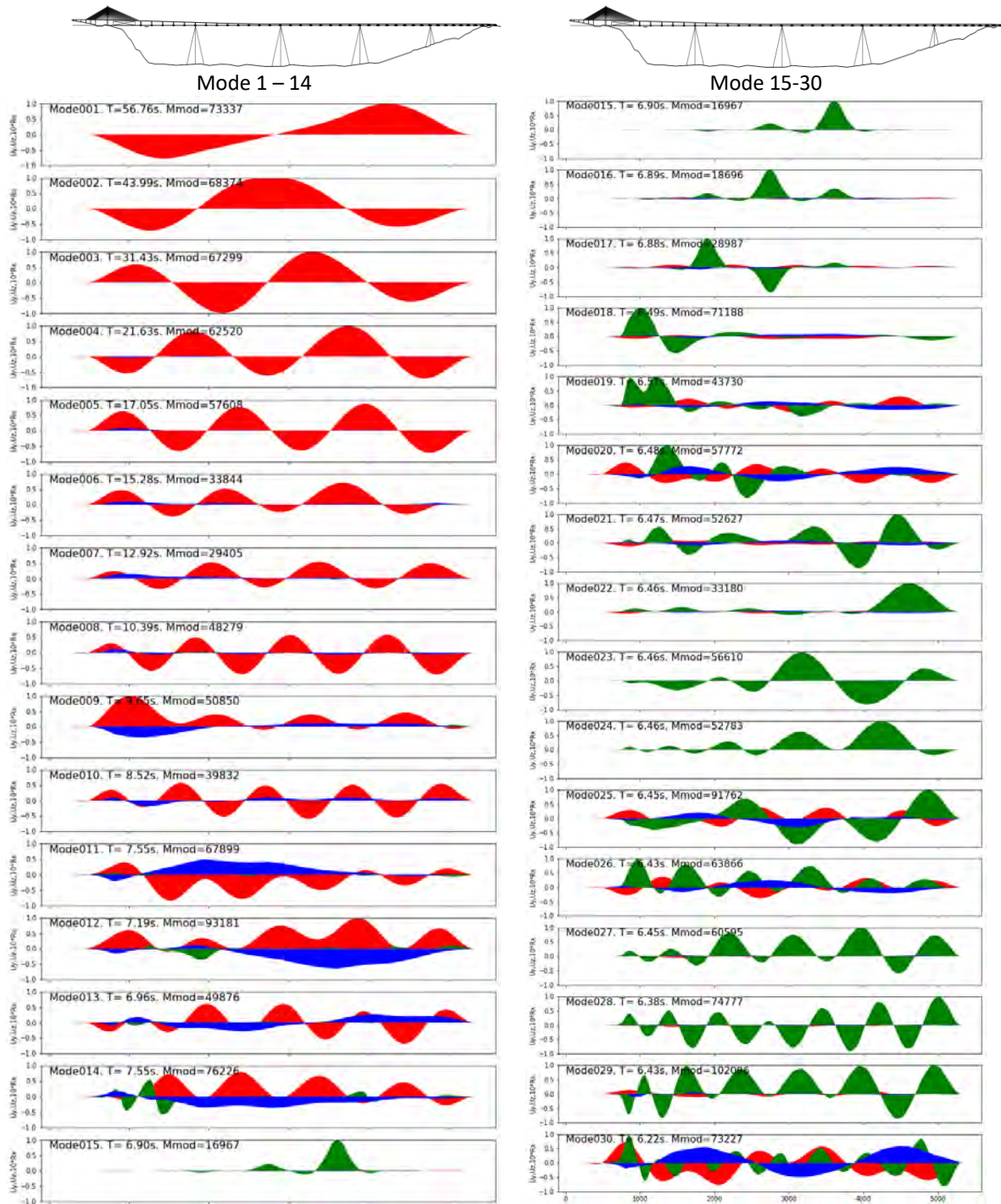


Figure 9 Modeplot of first 30 modes of K12_06. Red: Transverse direction, Green: Vertical direction. Blue: torsional component scaled by a factor of 10.

A comparison between the simplified method (blue line), time domain response calculations by Orcaflex and hand calculations is shown in Figure 10. As can be seen the agreement is fairly good. Further details are given in /13/.

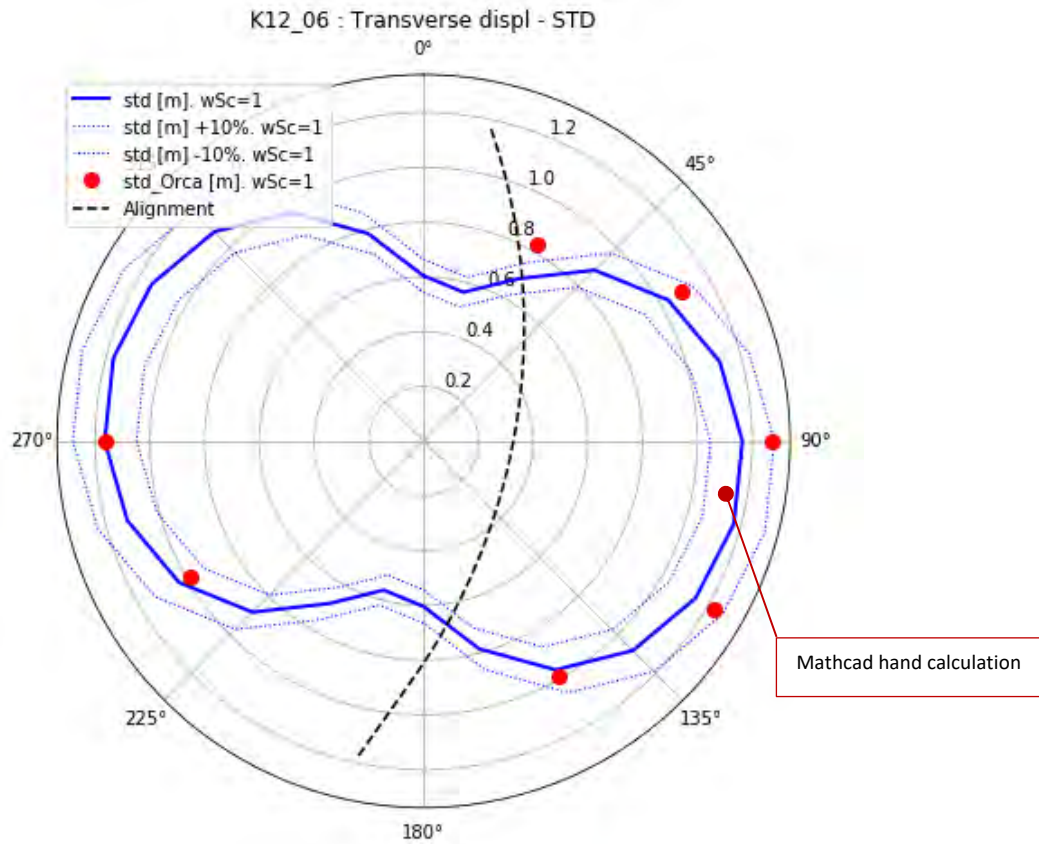


Figure 10 Comparison of standard deviation between simplified method and Orcaflex. Blue solid line: Simplified method. Blue dotted lines: Simplified method +/- 10%. Red dots: Orcaflex (average of 10 runs). Black broken line: Alignment of K12.

3.4 Inhomogeneity in wind - mean wind variation along the alignment

The Metocean Design Basis specifies a variation of mean wind speed as follows :

1. Constant.
2. Linearly varying from 0.6V at one end to V on the other.
3. Linearly varying from 1.0 at one end to 0.6 on the other.
4. Linearly varying from 0.8V at one end, V in the middle and 0.8 at the other end.

The variations are illustrated in Figure 11.

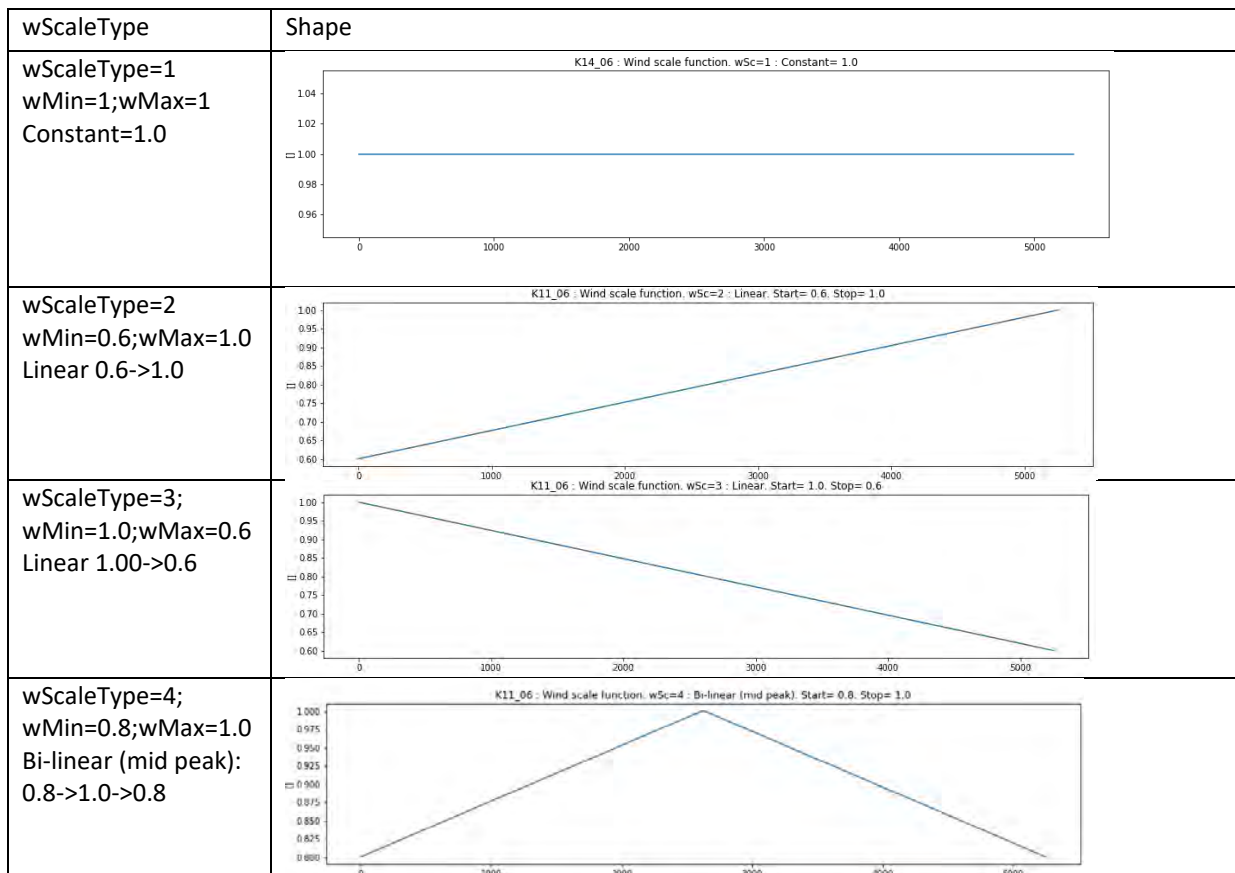


Figure 11 Wind variation along the alignment.

A summary of dynamic results for these mean wind variations is shown in Figure 12. As can be seen the general trend is that constant mean wind (Wind Scale Type 1) gives the highest dynamic response regardless of direction. Second largest effect is from Wind Scale Type 4. Both these cases are symmetric about the mean. The two remaining Wind Scale Types are un-symmetric, and the maximum of the two is dependent on the direction of the wind in relation to the structure.

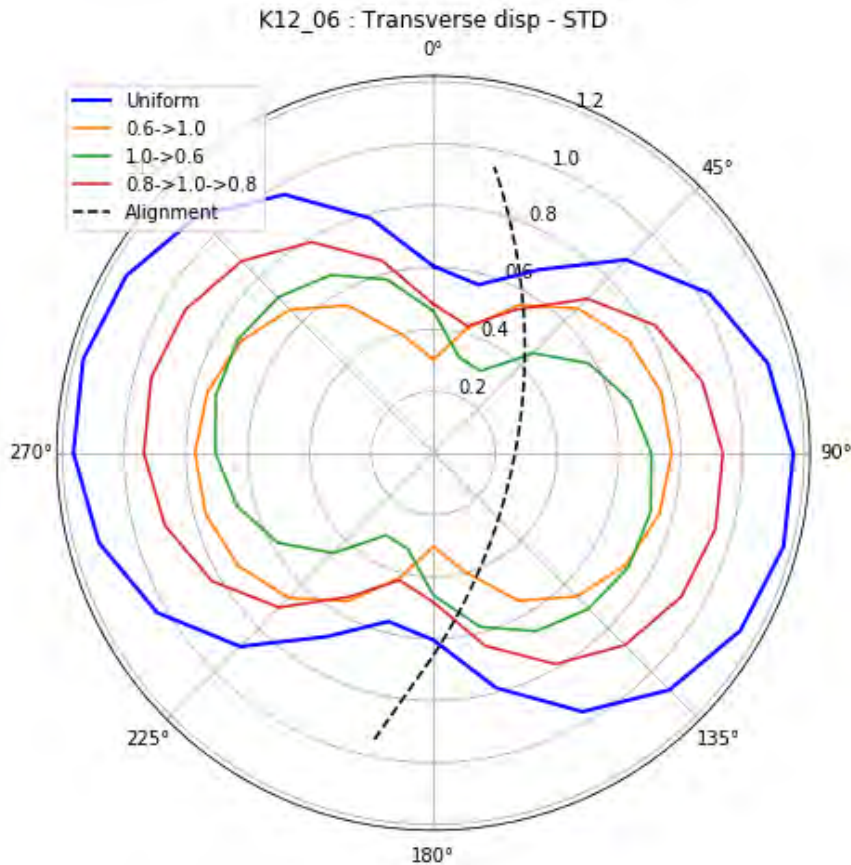


Figure 12 Dynamic response from varying mean wind profile along the deck, see Figure 11. The variation is from south towards north. I.e. for the yellow line the mean wind varies from 0.6 in the south to 1.0 in the north.

3.5 Effects of varying wind parameters.

In Metocean Design basis /2/ Table 15 indicate that parameters in the wind varies (see also Table 3). The key parameters are presented as P-values, representing probability of occurrence lower than the specified value. In order to understand the effect of the variation several relevant parameters were calculated and compared to the reference value; uniform wind as documented in Section 3.3.

Table 5 Extract from "Table 15". Input varied below marked with blue. *Cux not given in N400. ESDU value is used in reference calculations.

	Metocean Design Basis				Analysis input (z=10m) (scaled based on N400)		
	N400	P10	P50	P90	P10	P50	P90
z [m]	10,0	50,0	50,0	50,0	10,0	10,0	10,0
xLu [m]	100,0	108,0	232,0	586,0	66,6	143,2	361,6
xLv [m]	25,0	50,0	141,0	472,0	30,9	87,0	291,2
xLw [m]	8,3	21,0	40,0	81,0	13,0	24,7	50,0
Au	6,8	3,80	7,30	16,30	3,8	7,3	16,3
Av	9,4	5,60	13,30	32,50	5,6	13,3	32,5
Aw	9,4	7,70	12,30	18,20	7,7	12,3	18,2
Cux*	3,0	-	-	-	5,0	7,0	10,0
Cuy	10,0	6,40	9,00	10,8	6,40	9,00	10,8

The wind parameters varied is marked with blue lines in Table 5. P10, P50 an P90 is calculated and compared to the N400 reference values and given as the thick blue line in Figure 10. In addition to the thick blue reference line a +/- 10% is marked for reference. Figure 13 shows a summary of the standard deviation of the transverse response for the cases analyzed.

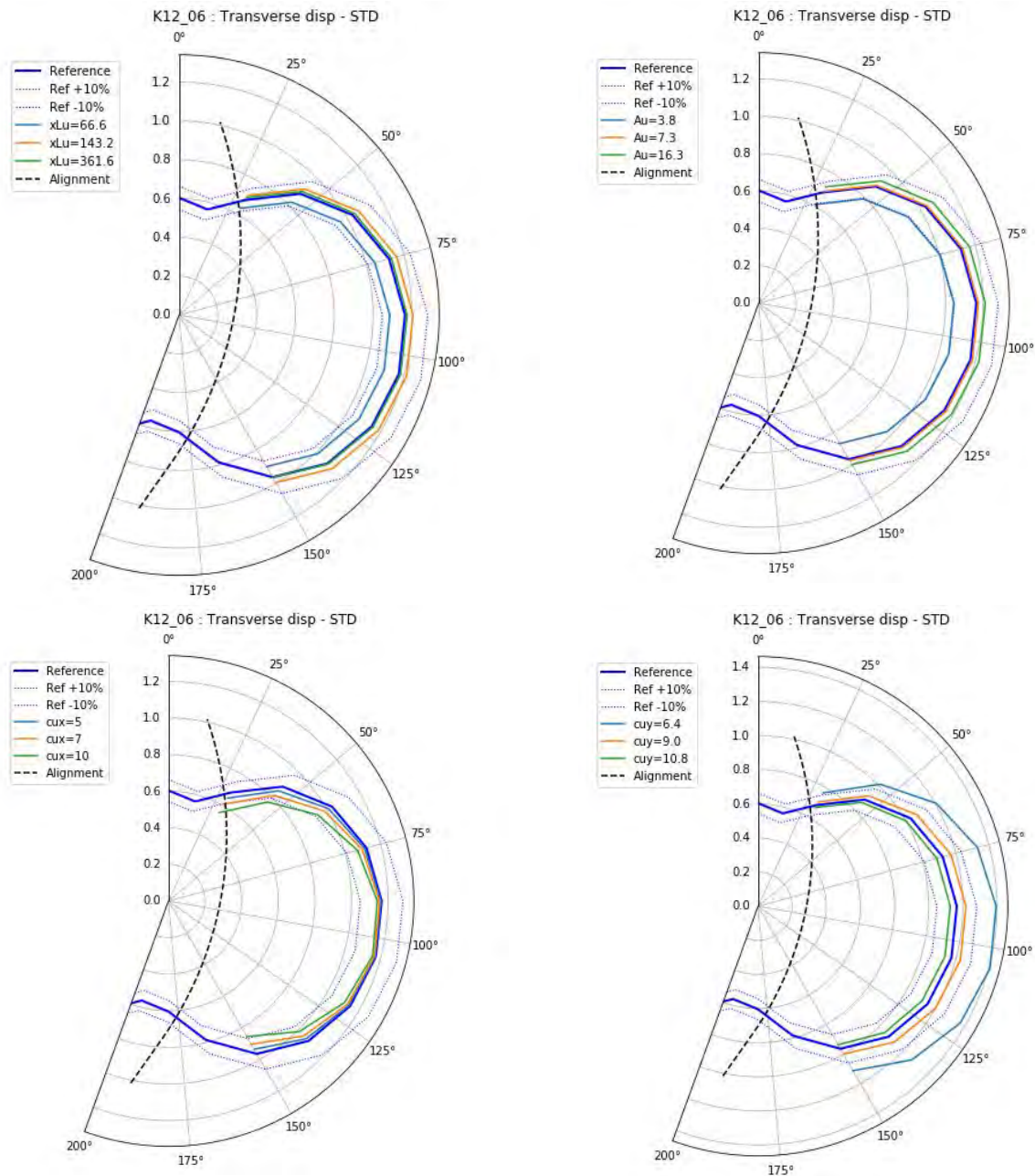


Figure 13 Top Left: Variation of xLu . Top Right: Variation of Au . Bottom left: Variation of cux . Bottom right. Variation of cuy

For variation of xLu the response follows the reference value within +/- 10%. Low and high xLu values give lowest response. The results indicate that the highest response value for this concept is for an xLu value in medium range.

For variation of Au the response follows the reference value within +/- 10%. The general trend is that increased Au values gives increase response.

For variation of C_{ux} the response follows the reference value within +/- 10%. The effect of change of c_{ux} is small for wind perpendicular to the alignment and more pronounced as the wind comes along the alignment. The C_{ux} value of 3.0 used in the reference case gives the highest value of the calculated cases and increase of C_{ux} value give reduced response.

For C_{uy} it can be seen that the response is sensitive to changes of this parameter, particularly for wind perpendicular to the alignment. Lower value of C_{uy} gives higher response, and C_{uy} values below the P10 value of 6.4 will increase the response with more than 20%. For skew wind, where the wind is more along the alignment, the effect is less pronounced.

4 Aerodynamic stability

4.1 Introduction – evaluation of bridge girder aerodynamic properties.

Following criteria set forward in N400 /3/ the bridge is considered to be in wind load class III. Hence verification of the wind stability of the bridge structure shall include interactions between the dynamics of the structure and wind field as well as aerodynamic stiffness and damping effects. The verification thus includes assessment of vortex induced vibrations as described in N400, section 5.4.3.7 /3/ and check of aerodynamic instabilities as described in N400 section 5.4.3.8 /3/.

Based on N400 the critical wind speed for onset of aerodynamic instability is 81.7 m/s. Detailed calculations are found in /14/.

Table 6 Steady state wind load coefficients for the K12 cross section from discrete vortex simulations /16/, used in the stability analysis.

C_{D0} [-]	C_{L0} [-]	$dC_L/d\alpha$ [1/rad]	C_{M0} [-]	$dC_M/d\alpha$ [1/rad]
0.675	-0.413	3.122	0.012	0.916

The wind load coefficients in Table 6 above are normalized the conventional way by the dynamic head of the wind $\frac{1}{2}\rho V^2$ and a characteristic dimension of the cross section. The section depth $H = 4.0$ m in case of the along wind drag loading and the cross section width $B = 30.2$ m in case of the lift and overturning moment. Please note that these values differs slightly from the values used in the integrated analysis.

The simulated aerodynamic derivatives shown in Figure 6 display the expected behaviour for non-dimensional wind speeds in the range $4 < V/fB < 18$ displaying a monotonic growth in a linear or parabolic fashion. For the highest non-dimensional wind speeds $18 < V/fB < 30$ it is noted that the $H_{2.4}^*$ and $A_{2.4}^*$ aerodynamic derivatives displays an unexpected non-monotonic behaviour which may influence stability calculations slightly, see Figure 6.

4.2 Vortex induced vibrations.

Vortex shedding in the wake of box girders may result in limited amplitude oscillations of the bridge girder at wind speeds where rhythmic vortex shedding locks on to a vertical bending or torsion eigen mode.

Practical experience from suspension bridges with shallow trapezoidal box girders have shown that vortex induced oscillations are usually confined to vertical modes only and occur at low wind speeds typically less than 12 m/s and for weather conditions with low atmospheric conditions.

Vortex induced vibrations of suspension bridges (Osterøy bridge, Norway and Storebælt East bridge, Denmark) has proven to be linked to severe flow separation and associated rhythmic vortex shedding at the knuckle line between the horizontal bottom plate and the lower inclined downwind side panel.

Wind tunnel research /5/ has demonstrated that severe flow separation and vortex shedding can be avoided if the angle between the horizontal bottom plate and the lower side panels can be kept at approximately 15 deg. The 15 deg principle was recently introduced for the design of the girder of the Hålogaland Bridge, Norway and has proven to be free of vortex induced vibrations in full scale as well as in wind tunnel tests.

The design of the cross section shape of the girders of Bjørnafjorden bridge incorporates the 15 deg. principle. Thus, vortex induced vibrations are not expected to be an issue for the present design.

In addition the Scruton number was assessed for each mode. Normally vortex shedding is not expected for modes with $Sc > 50$.

$$S_c := \frac{2 \cdot \delta_s \cdot m_e}{\rho \cdot b^2}$$

The calculation has been performed with modal structural, viscous and hydrodynamic damping. Aerodynamic damping is conservatively set to zero. The Scruton numbers are found to be above 100 for all checked modes. Thus, vortex shedding is not expected to be a problem for the bridge system.

4.3 Verification of aerodynamic instability

N400 specifies that a wind load class III bridge shall be verified for four types of aerodynamic instabilities:

- Galloping
- Static divergence
- Classical flutter
- Torsion instability

Each type of aerodynamic instability will be discussed in separate sections below.

4.3.1 Galloping

Galloping is a cross wind vertical instability resulting in onset of vertical divergent oscillations above a certain threshold wind speed.

A necessary condition for galloping to occur is that the lift slope $(dC_L)/d\alpha$ is negative. With reference to Table 3.1 $(dC_L)/d\alpha = 3.122 > 0$, thus galloping will not occur for the K12 design for Bjørnafjorden bridge.

4.3.2 Static divergence

Static divergence is a buckling type instability of the bridge girder occurring at the wind speed where the wind induced external moment acting on the girder exceeds the structural capacity. An estimate of the wind speed for onset for divergence V_{div} is given as /3/:

$$V_{div} = 2\pi f_\alpha \sqrt{\frac{2I_{\alpha eq}}{\rho B^4 dC_M/d\alpha}}$$

Where:

f_α is the eigenfrequency of the lowest torsion mode having modal mass M_α .

$I_{\alpha eq} = \frac{M_\alpha}{\int_0^L \varphi(x)^2 dx}$ is the corresponding equivalent mass moment of inertia.

$\rho = 1.25 \text{ kg/m}^3$ is air density

B = over-all girder width

The lowest torsion mode of the bridge is mode 11 displaying one partial half wave along the low level floating bridge, Figure 14, having an eigenfrequency $f_\alpha = 0.139 \text{ Hz}$ and a modal mass $M_\alpha = 67.899 \cdot 10^6 \text{ kg}$.

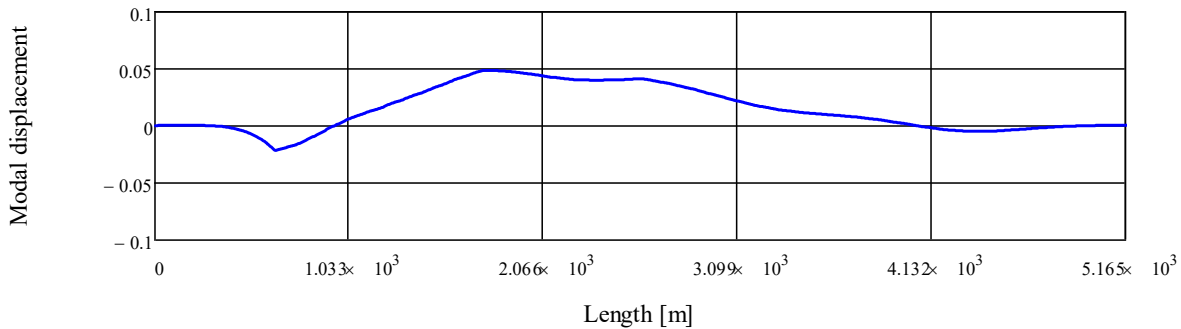


Figure 14 First torsion mode (mode 11) of Bjørnafjord K12 Alternative.

Inserting $dC_M/d\alpha = 0.916$ and the above structural properties in (4) a divergence wind speed $V_{div} = 174.9 \text{ m/s}$ which is well above the requirement of 81.7 m/s .

4.3.3 Classical flutter

Classical flutter involves as a minimum two modes of motion. A torsion mode and a vertical bending mode of similar mode shape but with a lower eigenfrequency. The critical wind speed for onset of classical flutter is reached when the wind loading on the bridge girder makes the bending and torsion frequencies equal thereby establishing a resonant exchange of energy between to two modes. This in turn leads to divergent coupled torsion bending oscillations of the bridge girder. In cases where more vertical modes exist below the torsion mode these vertical modes may couple to form a compound vertical mode shape which couples with the torsion mode at the onset of flutter.

The input to the flutter calculation constitutes the modes assumed to couple into flutter, the corresponding modal masses and eigenfrequencies and aerodynamic derivatives particular to the bridge deck.

The present multi-mode flutter analysis of Bjørnafjorden K12 alternative assumes that the first torsion mode and 9 vertical bending modes with frequencies lower than the torsional frequency may couple into flutter;

Torsional mode: 30.

Vertical modes: 15, 16, 17, 18, 19, 20, 21, 23, 25

Eigenfrequencies, modal shapes and modal masses with of the modes are given in Figure 9.

The mechanical damping of the bridge structure is an important parameter in flutter calculations as the requirement for onset of flutter is that the apparent aerodynamic damping exhausts the available mechanical damping. In the present context the mechanical damping available is obtained as the sum of the structural damping, the viscous damping, the hydrodynamic damping and the damping of the anchor lines. Aerodynamic damping is excluded as this component is included in the aerodynamic derivatives and varies as a function of wind speed.

The compound mechanical damping available in the bridge structure for the selected 10 modes are summarized in Table 7 from which it is noted that the lowest modal damping level is $\zeta = 0.0524$ obtained for mode 18 which is assumed as a conservative lower bound for the flutter calculations.

Table 7 Compound mechanical damping computed for the selected flutter modes.

	Mode 15	Mode 16	Mode 17	Mode 18	Mode 19
Damping [rel-to-crit]	0.0955	0.0950	0.0937	0.0524	0.1184
	Mode 20	Mode 21	Mode 23	Mode 25	Mode 30
Damping [rel-to-crit]	0.0966	0.1147	0.1160	0.1033	0.1545

Flutter diagrams showing the outcome of the 10 mode analysis are shown in Figure 15. The apparent damping level to be balanced by the aerodynamics is $g = 2\zeta = 0.105$, see section 6.

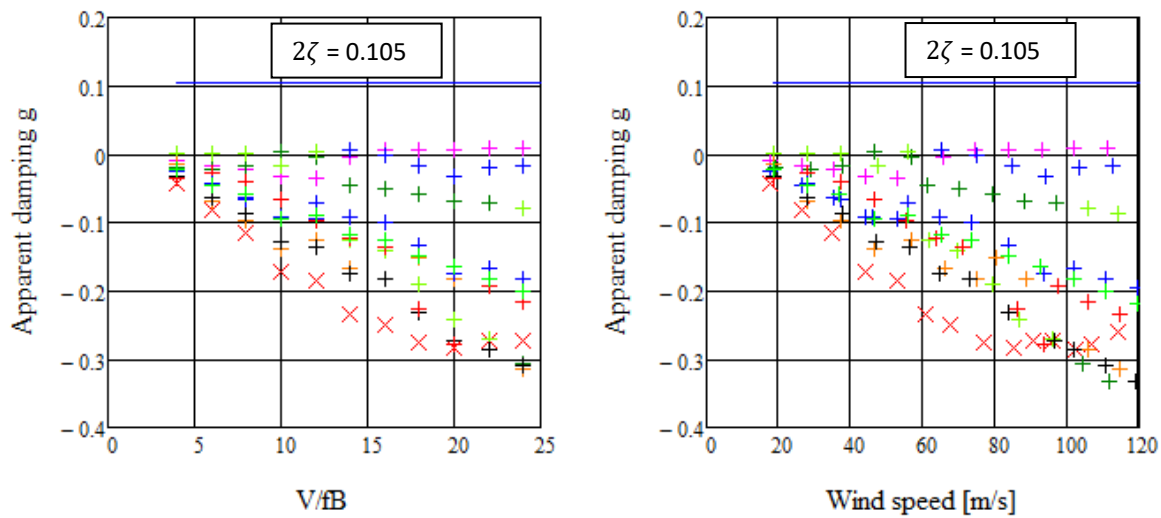


Figure 15 Apparent aerodynamic damping as function of normalized and absolute wind speed for $2\zeta = 0.105$ Bjornafjorden K12 alternative.

From Figure 15 it is noted that all apparent damping levels remain below $2\zeta = 0.105$ for all wind speeds below 120 m/s. Hence the bridge is stable against classical flutter up to and beyond the N400 requirement of 81.7 m/s. It is noted that slightly positive apparent damping is found for wind speeds above $V/fB > 10$ or 45 m/s which indicates onset of flutter had the compound mechanical damping been below 0.003 ($g = 0.006$) as may be the case for land based suspension bridges.

Further details about the calculations are given in /14/.

4.3.4 Torsion instability

Torsion instability is a condition resulting in onset of torsional divergent oscillations above a certain threshold wind speed. Torsion instability is associated with the formation and travel of large coherent vortex structures across the bridge deck. This type of instability is often associated with bluff plate girder bridge decks.

A necessary condition for the occurrence of torsion instability is that the A_2^* aerodynamic derivative change sign from negative at low wind speeds to positive at higher wind speeds.

From Figure 6 it is noted that A_2^* remains negative for all non-dimensional wind speeds up to at least $V/fB = 30$. It may thus be concluded that Bjørnafjorden K12 alternative will not encounter torsion instability at wind speeds below a wind speed of $30 \cdot f_{\alpha} B = 125.9$ m/s which is well above the N400 requirement.

4.4 Evaluation of flutter coefficients used

An evaluation of the flutter coefficients used above has been performed, see /12/. This is done by pairing the calculated flutter coefficients for SS1-b with the Storebælt East bridge data. The geometry of the Storebælt East bridge and the K12 cross section is not identical, thus a perfect match of the above flutter calculation and the Storebælt wind tunnel tests cannot be expected. However, the relatively close match is quite satisfactory and supports the credibility of the computed aerodynamic derivatives.

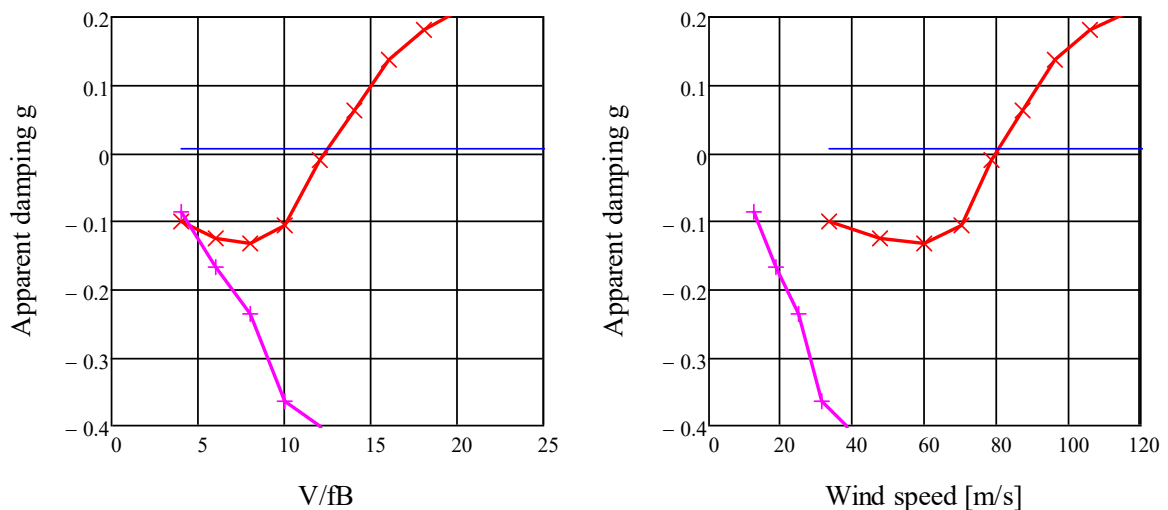


Figure 16 Determination of the critical wind speed for onset of flutter in non-dimensional form(left) and actual wind speed (right). Example: Storebælt East Bridge dynamic properties paired with K12 aerodynamic derivatives.

4.5 Tower

The concrete tower is heavy and of limited height. Thus, it is not expected to show problems with vortex shedding or instabilities.

4.6 Vibration of cables in the cable stayed bridge.

4.6.1 Introduction

This section summarizes the findings regarding cable vibrations in the cable stayed bridge for the following topics:

The following aerodynamic cable instabilities has been evaluated below:

- Dry galloping – an instability associated with asymmetric flow separation on the cable cross sections. The asymmetry may be caused either by the cable being in the critical Reynolds number range or by cable surface irregularities.
- Ice / sleet galloping – an instability associated with the deposit of ice, snow or sleet along the cables causing the circular cable cross sections to be asymmetric to the wind.
- Rain / wind galloping – an instability associated with rain water draining along the cables causing the circular cable cross sections to be asymmetric to the wind.
- Vortex induced vibrations – an instability associated with the alternating formation and shedding of vortices along the separation lines at the upper and lower sides of the stay cable.

Common to the above instabilities are that they may be mitigated or delayed to higher wind speeds by introduction of additional mechanical damping to the stay cables. Further details are given in /15/.

4.6.2 Dynamic properties and external damping for cables.

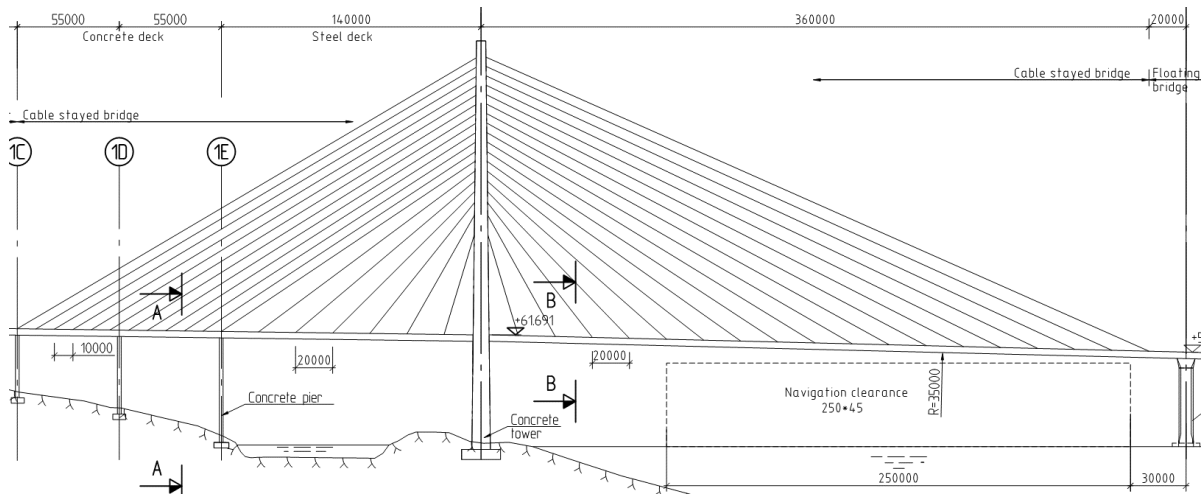


Figure 17 Cable stayed bridge of the Bjørnafjorden K12 alternative.

Figure 17 shows the general arrangement of the cable stayed bridge part. The cables are of a fan type and supports a main span of about 360m. Based on the current geometry the vibration frequency can be calculated. The lowest frequency varies from about 0.3Hz for the longest stays to 1.7Hz for the shortest. The distribution is shown in Figure 18.

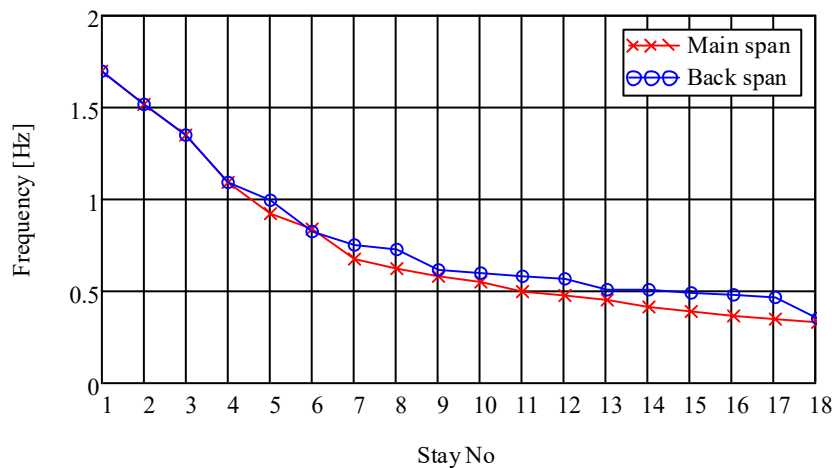


Figure 18 Lowest vibration frequency of each stay.

For cable stayed bridges it is expected that additional damping in some form is needed to damp out cable vibrations. Figure 19 shows an example of one such system. The typical damping obtained from a system like this is 275 kNs/m, which for the current cables equates to an additional damping of about 2% of critical, see Figure 20.

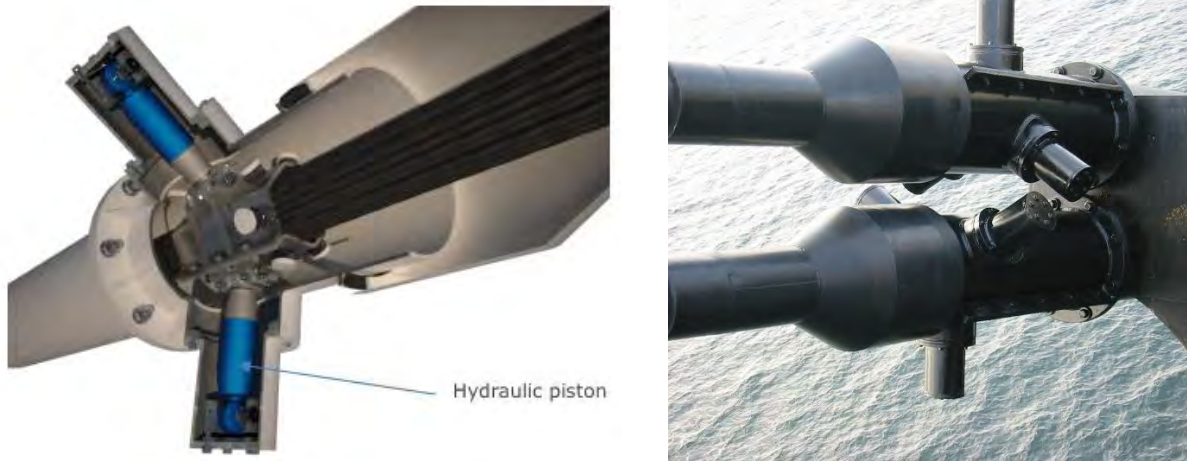


Figure 19 Hydraulic stay cable damper (Freyssinet IRD type). Cross section view (left). External view twin stay cables, Øresundsbron [right].

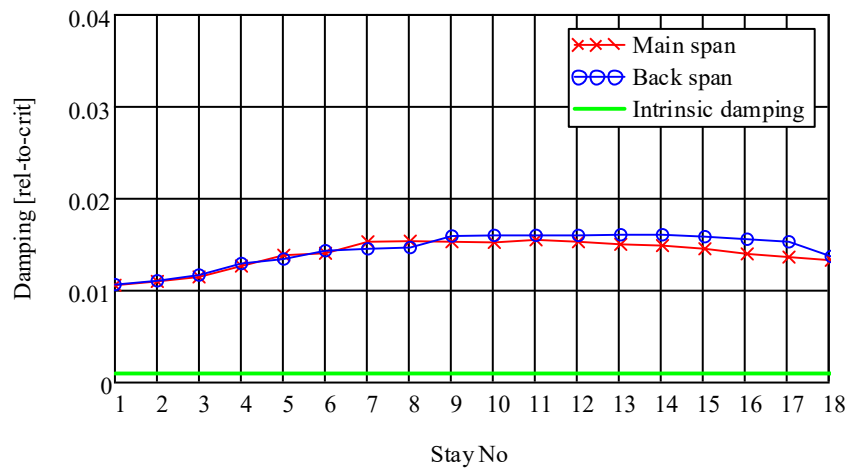


Figure 20 Estimated mechanical first mode damping of the main and back span stay cables

4.6.3 Dry galloping

Dry galloping may occur as the wind flow about an inclined stay cable enters the critical Reynolds' Number range ($2 \cdot 10^5 < Re < 3.5 \cdot 10^5$). In this range the drag coefficient C_D drops from a nominal value of 1.2 to approximately 0.4 while a distinctive cross-wind lift coefficient C_L may develop ($C_L \approx \pm 0.4$) due to asymmetric formation and location of the upper and lower separation lines along the cable.

The action of the Re dependent lift and drag forces produces a quasi-steady aerodynamic force in the direction of cable movements and thus a resulting negative aerodynamic damping which must be balanced by structural damping if cable movement is to be prevented.

The cable amplitudes due to dry galloping once started cannot be predicted. However, the critical wind speed and the damping necessary for prevention can be estimated and is discussed in detail in /15/

The critical wind speeds V_{CG} for dry galloping of the main and back span cables are calculated from the critical Reynolds' Numbers $Re_{max} = 3.3 \cdot 10^5$, $Re_{max} = 1.6 \cdot 10^5$ yielding maximum galloping excitation in smooth and turbulent flow:

$$V_{CG} = \frac{Re_{max}v}{b}$$

The estimated dry galloping wind speeds for the main and back span stay cables and intrinsic damping only, are shown in Figure 21 along with the EN1991-1-4 galloping criterion (1.1).

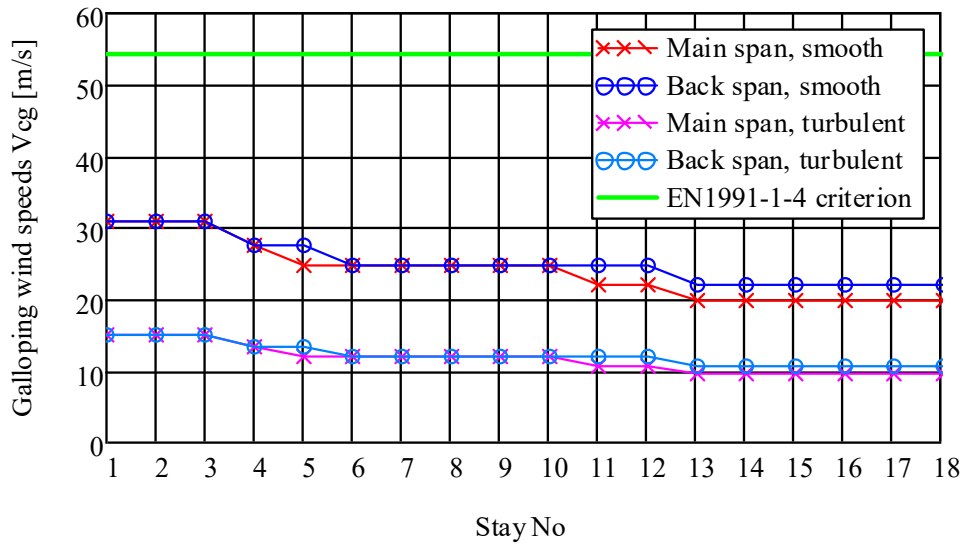


Figure 21 Calculated critical wind speeds for maximum dry galloping excitation of all cables in smooth flow.

As can be seen from Figure 21 galloping is expected in smooth flow if additional damping sources is not taken into account. If aerodynamic damping on the cables is included as described in /15/, it can be seen that additional damping is still needed to suppress dry galloping for smooth flow, see Figure 22.

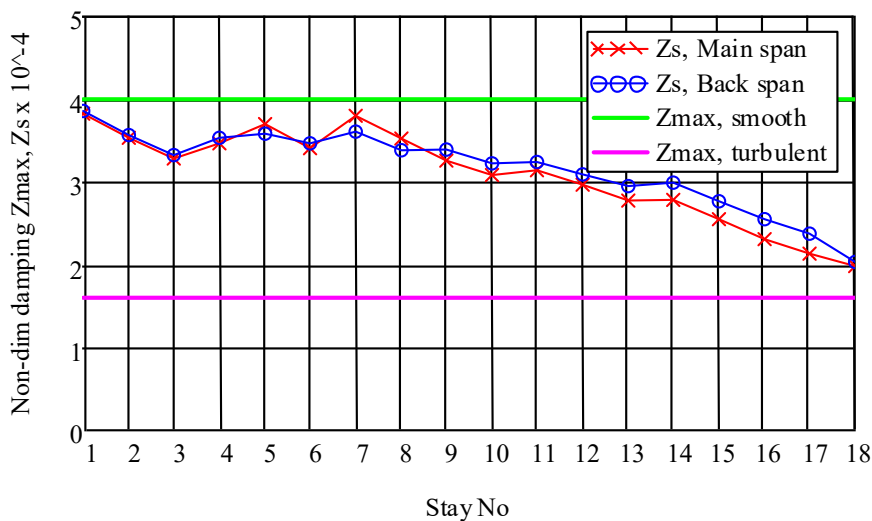


Figure 22 Calculated total damping of stay cables compared to required non-dimensional damping(Z) for smooth and turbulent flow to suppress dry galloping.

4.6.4 Galloping from surface irregularities of HDPE tube

New research into the galloping of cylindrical cable surface elements has revealed that small deviations from the perfect circular cross section shape may cause substantial cross wind lift forces in

the critical Reynolds number range $2 \cdot 10^5 < Re < 3.5 \cdot 10^5$. Wind tunnel measurements of the lift and drag coefficients as function of Re with the inflow angle α as parameter for a commercial HDPE tube having a diameter of 160 mm with ± 1 mm deviations is shown in Figure 23 (See /15/ for proper referencing).

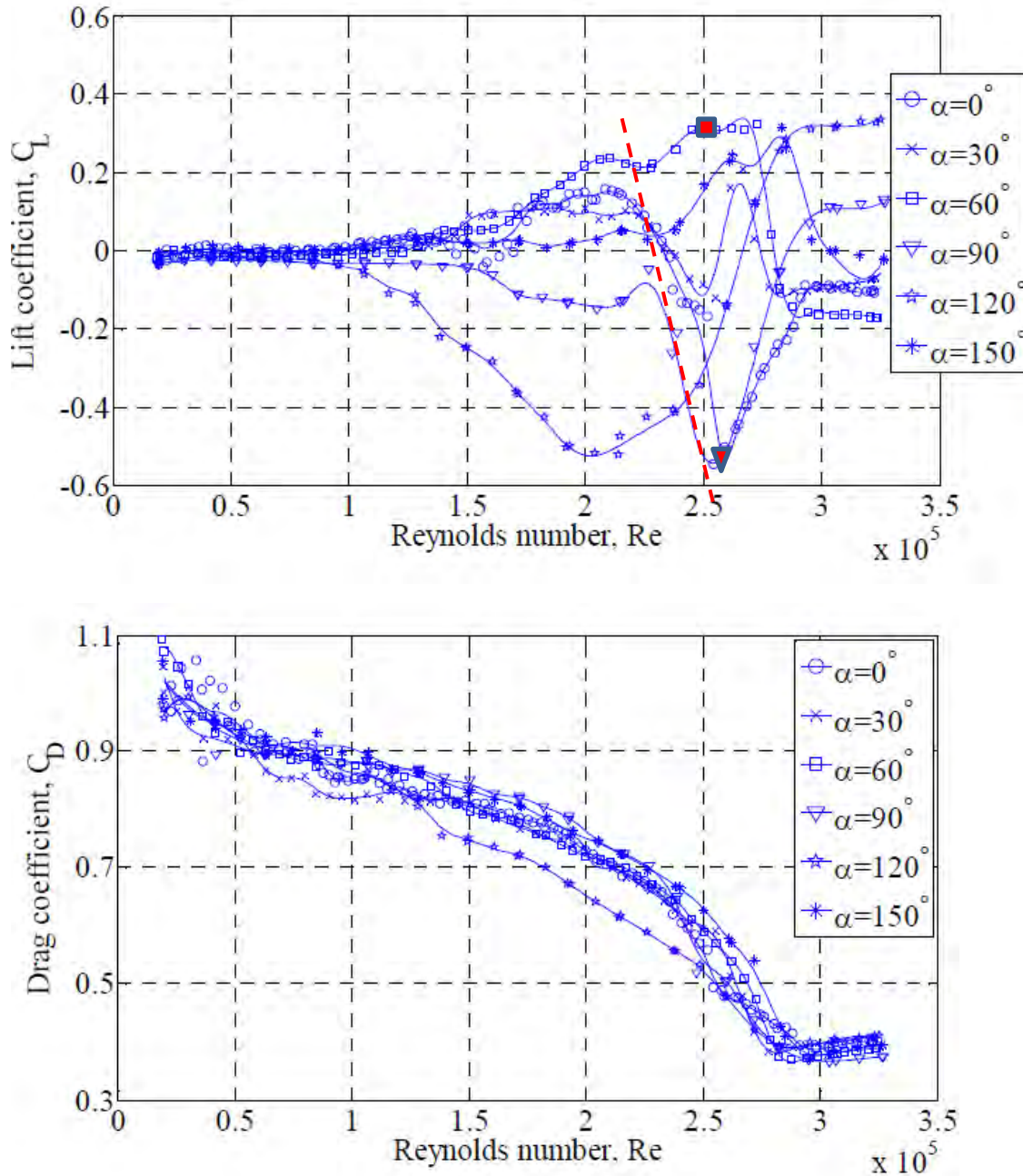


Figure 23 Variations of lift (upper) and drag (lower) coefficients as function of Re and inflow angle α for a commercial stay cable HPDE tube. See /15/ for proper referencing.

From the figures two different sources of galloping can be possible: Classical den Hartog galloping due to a negative lift coefficient gradient as function of inflow angle, and dry galloping due to a negative gradient of the lift coefficient due as function of the Reynolds number.

The estimate non-dimensional damping parameter needed to damp the aerodynamic excitation arising from surface imperfection can be calculated to about $2.72 \cdot 10^4$. See /15/ for further details

regarding calculations. Figure 24 compares this to the damping for each cable when including aerodynamic damping and external damper units. As can be seen the damping seems not to be satisfactory for stays 15-18. However, the method used for calculation the necessary damping is likely to be conservative, as the evaluation is based on a worst case estimate (one section of the cable and one inflow angle only). More elaborate evaluations based on wind tunnel tests dedicated to the actual cable HPDE pipes are expected to produce lower and more favourable damping estimates.

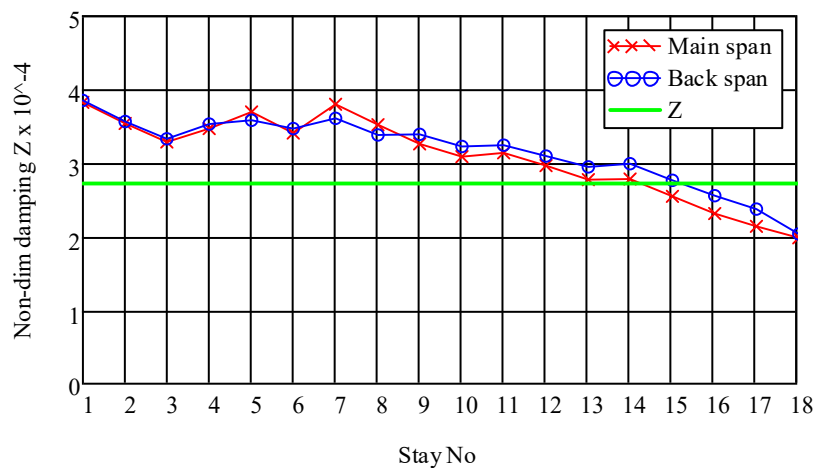


Figure 24 Calculated non-dimensional cable damping parameters for the main and back span cable stays including damper units and comparison to the aerodynamic non-dimensional damping necessary to suppress aerodynamic excitation arising from surface imperfections.

4.6.5 Rain/wind galloping

The method derived from observations of rain-wind induced vibration of Erasmus bridge in Rotterdam has been used to evaluate this effect (See details in /15/). When estimating maximum cable vibrations due to rain / wind galloping of the cables without dampers an expected amplitudes in the range 0.5 m – 3.0 m is found. This exceeds the criteria of about 0.2m. When including the mechanical dampers all cables are predicted to be stable against rain / wind galloping, $a \approx 0$.

4.6.6 Ice/sleet galloping

EN1991-1-4, Table E.7, proposes that galloping due to ice / sleet deposits is a similar process to classical den Hartog galloping and is caused by the change of the exterior cable surfaced due to ice accretion. For evaluation it may be represented by the stability parameter $a_G = 1$. However, contrary to dry galloping discussed in the previous section the aerodynamic force coefficients and thus a_G are assumed to independent of wind speed and thus also of the Reynolds' Number.

Based on the same calculation method as in 4.6.3 Dry galloping, where both aerodynamic and external dampers is included, it is found that the cables are stable for this phenomena for wind speeds up to 15 m/s, see Figure 25. The values presented in this figure is valid for cables with ice/sleet along the whole length. If ice accretion is restricted to a limited part of the cable the galloping excitation will be less and in part counterbalanced by positive aerodynamic damping along the parts of the cables free of ice / sleet.

In /15/ a method is presented for evaluating the stability with the cable partly covered by ice/sleet. Based on this analysis the cable will be stable for wind speeds above 54m/s when the cable is iced up less than 22% of its length.

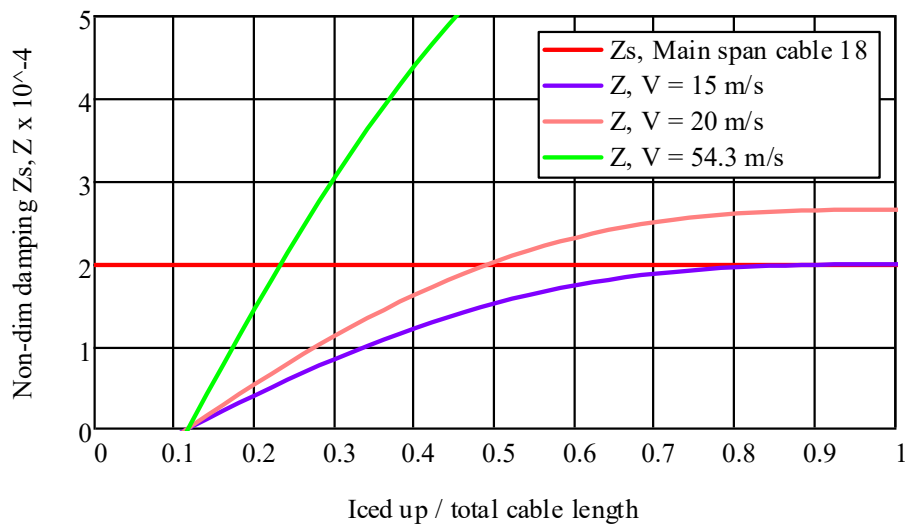
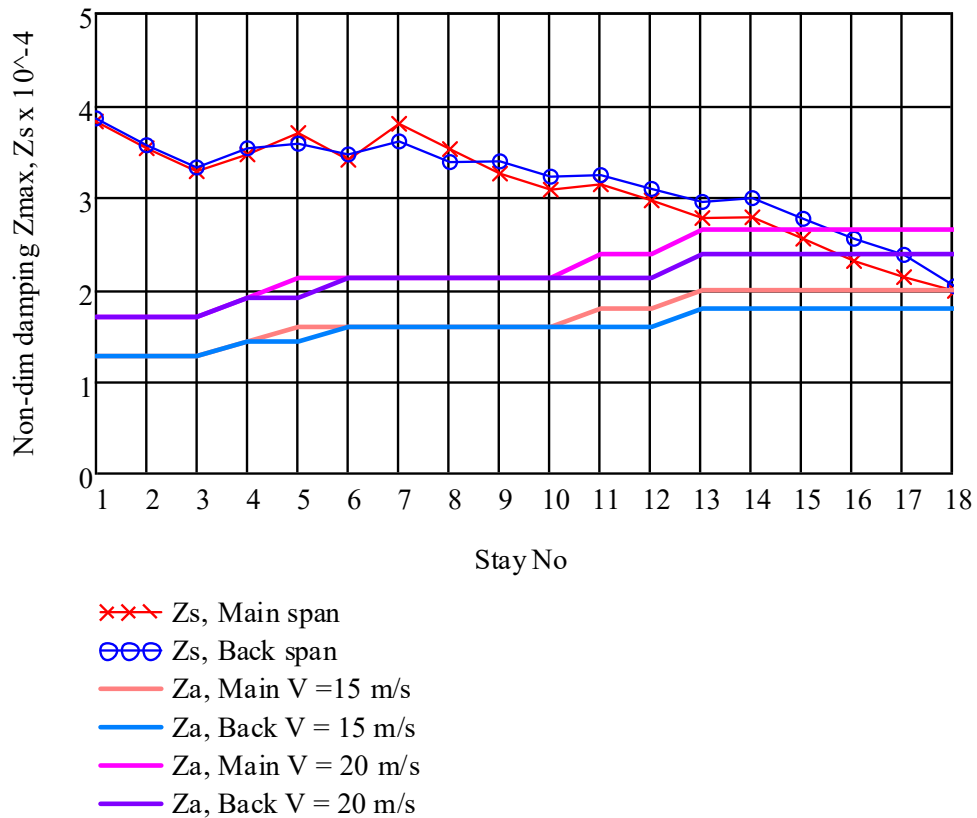


Figure 25 Top: Calculated non-dimensional structural cable damping parameters Z_s and aerodynamic damping parameters Z corresponding to ice / sleet galloping at wind speeds 15 m/s and 20 m/s. Bottom: Evaluation stability based on relative length of ice/sleet coverage.

4.6.7 Vortex induced vibrations

Vortex shedding excitation of a stay cable may occur when the frequency f_{vtx} of vortices shed in the wake of the cable coincides with one of the eigenfrequencies f_n of the cable, $f_v = f_n$.

Following EN1991-1-4 the vortex shedding frequency is related to the wind speed and cable cross section diameter b through the Strouhal Number ($St=b*f/V=0.18$). Thus, critical wind speed for the stays are calculated to 1.5m/s for the shortest stays to 0.5m/s for the longest.

Proceeding with calculations according to method 1 in EN1991-1-4 it is found that higher modes are more critical than lower, and that dampers are necessary if vortex induced vibrations occur. Figure 26 shows that vortex induced vibrations is suppress with dampers installed.

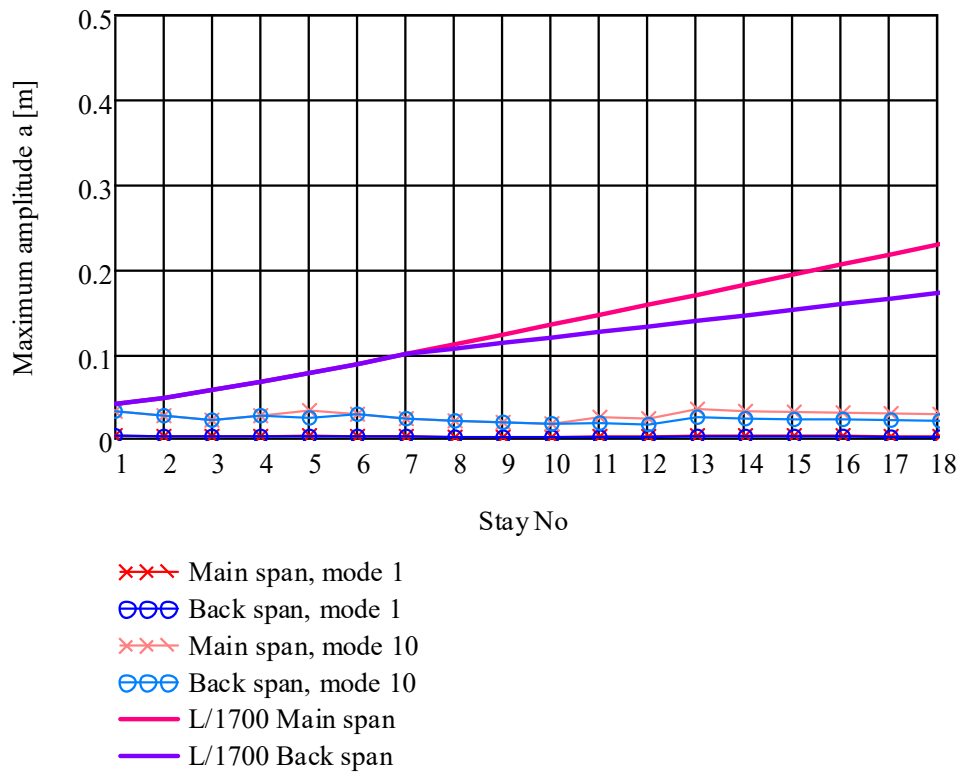


Figure 26 Estimated response of vortex induced vibration with dampers installed.

5 Other wind related issues

5.1 Bridge closure due to wind

In previous phases of the Bjørnafjorden project it has been concluded that the bridge availability is above 99.5%. The main contributor to bridge closure is closure due to wind on vehicles. In the updated Metocean Design Basis specified for this project /2/ the turbulence intensity from the southern sector is increased from about 12% to 30%. This implies a significant increase in wind gust compared to the mean wind speed, and thus, increased transverse forces acting on vehicles passing this sector of the bridge. In particular, vehicles will be negative affected by wind having its main direction from it side.

Figure 27 shows the wind rose, sector with increased turbulence and the different alignments. As can be seen, vehicles on K11 and K12 will experience side wind when passing the southern sector. In order to secure safe passage of these vehicles, mitigations may be needed. This could be e.g. closing the bridge for lower mean wind speed (this will have a considerable effect on the availability), establishing wind screens or other measures.

Before starting exploring the consequences of mitigation we recommend to:

- Look at the wind measurements to see if the turbulence intensity can be reduced or the width of the sector with increased turbulence intensity can be specified in more detail.
- Do more detailed analysis on bridge closure. For these analysis Weibull parameters for long term distribution is needed for all sectors.

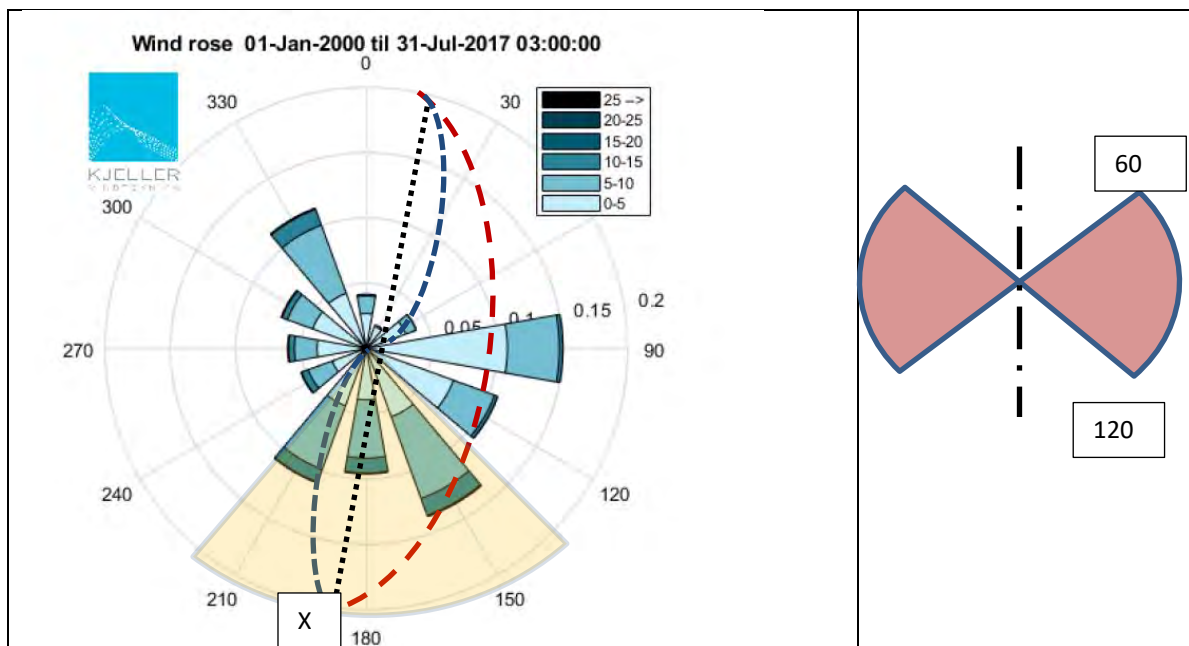


Figure 27 Left: Wind rose and area of increased turbulence intensity (Yellow), compared to K12 (Red), K13 (Black) and K14 (Blue). Right: Critical wind direction compared to alignment (red).

6 References

- /1/ SBJ-32-C4-SVV-90-BA-001 - Design Basis Bjørnafjorden.
- /2/ SBJ-01-C4-SVV-01-BA-001 - Metocean Design Basis.
- /3/ N400: Håndbok, Bruprojektering, Statens vegvesen
- /4/ SBJ-32-C4-SOH-20-RE-001 - Wind model testing for floating bridge, small-scale test, step 1
- /5/ NS-EN 1991-1-4:2005+NA:2009. Eurocode 1: Action on structures. Part 1-4: General actions – Wind actions
- /6/ 10205546-08-NOT-016 AMC status 1 – Aerodynamic assessment
- /7/ 10205546-08-NOT-060-00 Aerodynamic load coefficients sensitivity
- /8/ 10205546-08-NOT-061-00 Wind load coefficients – Storebælt
- /9/ 10205546-08-NOT-062-00 CFD analysis of cross sections
- /10/ 10205546-08-NOT-068-00 Buffeting effects of inhomogeneity
- /11/ 10205546-08-NOT-098-00-Bridge Closure Due To Wind
- /12/ 10205546-08-NOT-176-00-Aerodynamic stability of K11
- /13/ 10205546-08-NOT-183-00-Inhomogeneity in wind – Effects on K12
- /14/ 10205546-08-NOT-184-00-Aerodynamic stability of K12
- /15/ 10205546-08-NOT-191-00-Cable vibrations of cable stayed bridge – K12
- /16/ 10205546-08-NOT-192-00-CFD Analysis of K12

7 Enclosures

Enclosure 01: Tower Load Coefficients during construction

Enclosure 02: 10205546-08-NOT-016 AMC status 1 – Aerodynamic assessment

Enclosure 03: 10205546-08-NOT-060-00 Aerodynamic load coefficients sensitivity

Enclosure 04: 10205546-08-NOT-061-00 Wind load coefficients – Storebælt

Enclosure 05: 10205546-08-NOT-062-00 CFD analysis of cross sections

Enclosure 06: 10205546-08-NOT-068-00 Buffeting effects of inhomogeneity

Enclosure 07: 10205546-08-NOT-098-00-Bridge Closure Due To Wind

Enclosure 08: 10205546-08-NOT-176-00-Aerodynamic stability of K11

Enclosure 09: 10205546-08-NOT-183-00-Inhomogeneity in wind – Effects on K12

Enclosure 10: 10205546-08-NOT-184-00-Aerodynamic stability of K12

Enclosure 11: 10205546-08-NOT-191-00-Cable vibrations of cable stayed bridge – K12

Enclosure 12: 10205546-08-NOT-192-00-CFD Analysis of K12